SUPPORTING INFORMATION TO:

Promoted Ceria: A Structural, Catalytic and Computational Study

Ramzi Farra,[a] Max García-Melchor,[b] Maik Eichelbaum,[a] Maike Hashagen,[a] Wiebke Frandsen,[a] Jasmin Allan,[a] Frank Girgsdies,[a] László Szentmiklósi,[c] Núria López,[b] Detre Teschner[a,]*

a Fritz-Haber-Institut der Max-Planck Gesellschaft, Faradayweg 4-6, D-14195 Berlin, Germany
b Institute of Chemical Research of Catalonia, Av. Països Catalans, 16, 43007 Tarragona, Spain
c Centre for Energy Research, Hungarian Academy of Sciences, Budapest, H-1525, Hungary

Table of Contents

1. Details to *in situ* PGAA

In situ Prompt Gamma Activation Analysis (PGAA) is a technique recently implemented for studying catalysts in action.[1] It is based on the radiative neutron capture of nuclei, enabling the quantification of most elements in the investigated volume, in our case, inside a Deacon micro-reactor. PGAA at atmospheric pressure condition was carried out at the cold neutron beam of the Budapest Neutron Centre. For the experiments, a quartz tube reactor was placed into the neutron beam, and the reactor tube was surrounded by a specially designed oven having openings for the incoming and outgoing neutrons and for the emitted gamma rays. These openings are covered by thin aluminium foils for decreasing heat losses. 0.25 g of doped and undoped CeO_2 with the sieve fraction of 0.1-0.315 mm was loaded into the reactor. Various gas feeds, at constant 166.7 cm^3 min^{-1} total flow, were supplied by mass flow controllers. HCl (4.5), oxygen (5.0) and nitrogen (5.0) were used. The standard reaction condition was set to O_2:HCl:N_2 = 9:1:0 at 703 K, and the reaction was monitored by iodometric titration. A Compton-suppressed high-purity germanium crystal was used to detect the prompt-gamma photons. Molar ratios, Cl/(Ce+M), (M: dopant) were determined from the characteristic peak areas corrected by the detector efficiency and the nuclear data of the observed elements.[2]

2. A typical LabMax protocol

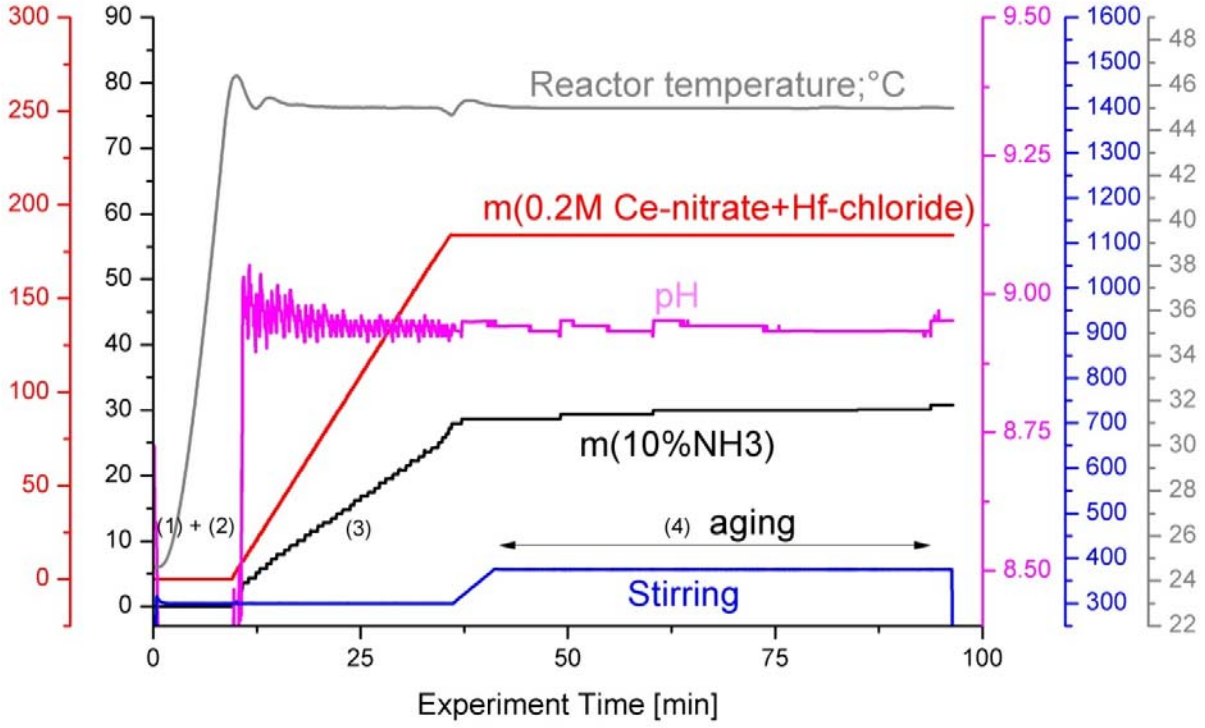

Figure S1. A typical LabMax® protocol on the example of the synthesis of $Ce_{0.95}Hf_{0.05}O_2$. The protocol reads as follows; (1) increasing the reactor temperature till 45 °C; (2) basification to pH = 8.95; (3) addition of metal salt solution (7 mL min^{-1}) while keeping the pH constant at 9 by adding appropriate amounts of ammonia solution (10 wt.%); (4) aging for 1 hour accompanied by increasing the rotation speed to 375 rpm.

3. Microwave conductivity setup, additional results

The setup for the *in situ* microwave cavity perturbation technique (MCPT) was described in detail earlier.[3] In short, a quartz tube plug-flow reactor with 4 mm outer and 3 mm inner diameter was placed in the center of a cylindrical X-band TM_{110} cavity resonating at 9.2 GHz. The reactor was connected upstream to a gas delivery manifold and downstream to a gas chromatograph. The reactor itself was inserted into an evacuated double-walled quartz dewar for heating of the sample by a preheated stream of N_2 without heating up the resonator. The temperature at the sample was controlled by a K-type thermocouple located inside the reactor. The resonator was kept at 20°C by external piezoelectric cooling elements. The conductivity of the sample was obtained by measuring the resonance curve in reflection mode with a vector network analyzer (Agilent PNA-L). The resonance frequency and quality factor of the resonator were deduced by an automatized parallel resonant circuit fit routine based on the transmission line theory.[4] From the difference of the reciprocal quality factors with and without sample the imaginary part of the powder permittivity $\varepsilon_{2,powder}$ was determined after the protocol described in Ref.3. The bulk permittivity $\varepsilon_{2,bulk}$ was calculated by applying the effective medium model after Landau-Lifshitz-Looyenga.[5] The microwave conductivity σ_e of the sample was calculated after $\sigma_e = \varepsilon_{2,bulk} \varepsilon_0 \omega_0$, with ε_0 being the vacuum permittivity and ω_0 being the angular resonance frequency of the empty resonator.

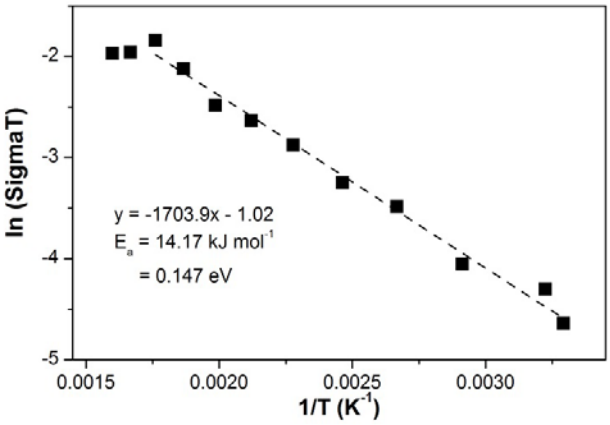

Figure S2. Ln(SigmaT) plot as a function of inverse temperature for CeHf-5, as deduced from the temperature dependent MW conductivity experiment.

4. Additional HCl oxidation results

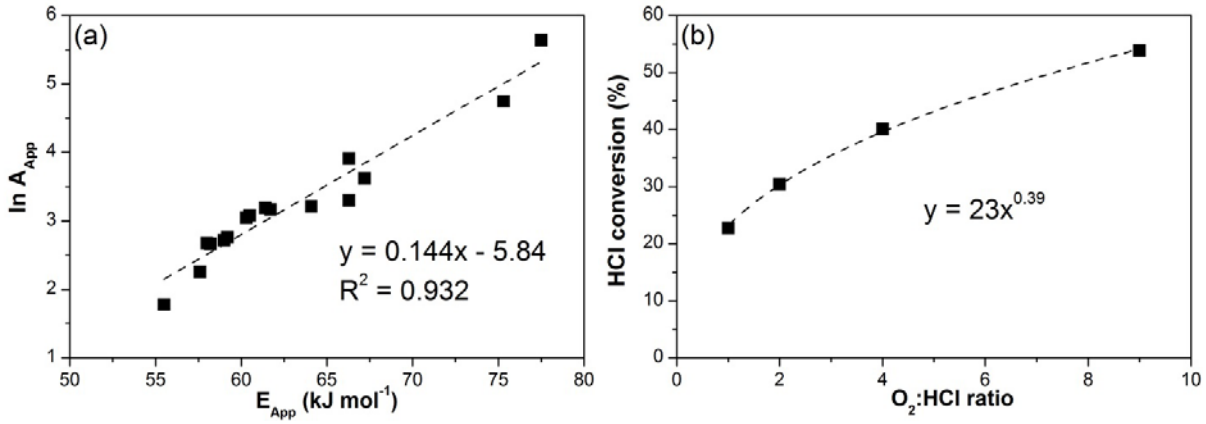

Figure S3. (a) Constable-Cremer relationship for HCl oxidation over doped and undoped CeO_2 catalysts. The Arrhenius parameters were determined in the temperature range of 643–703 K with a reaction mixture O_2:HCl:N_2 = 9:1:0 and a catalyst loading of 0.25 g. The rate was plotted as "mol Cl_2 g^{-1} min^{-1}" in the Arrhenius diagram. (b) Oxygen partial pressure dependence (at constant HCl and total flow rate) with CeHf-10 at 703 K.

5. Detailed CO oxidation results

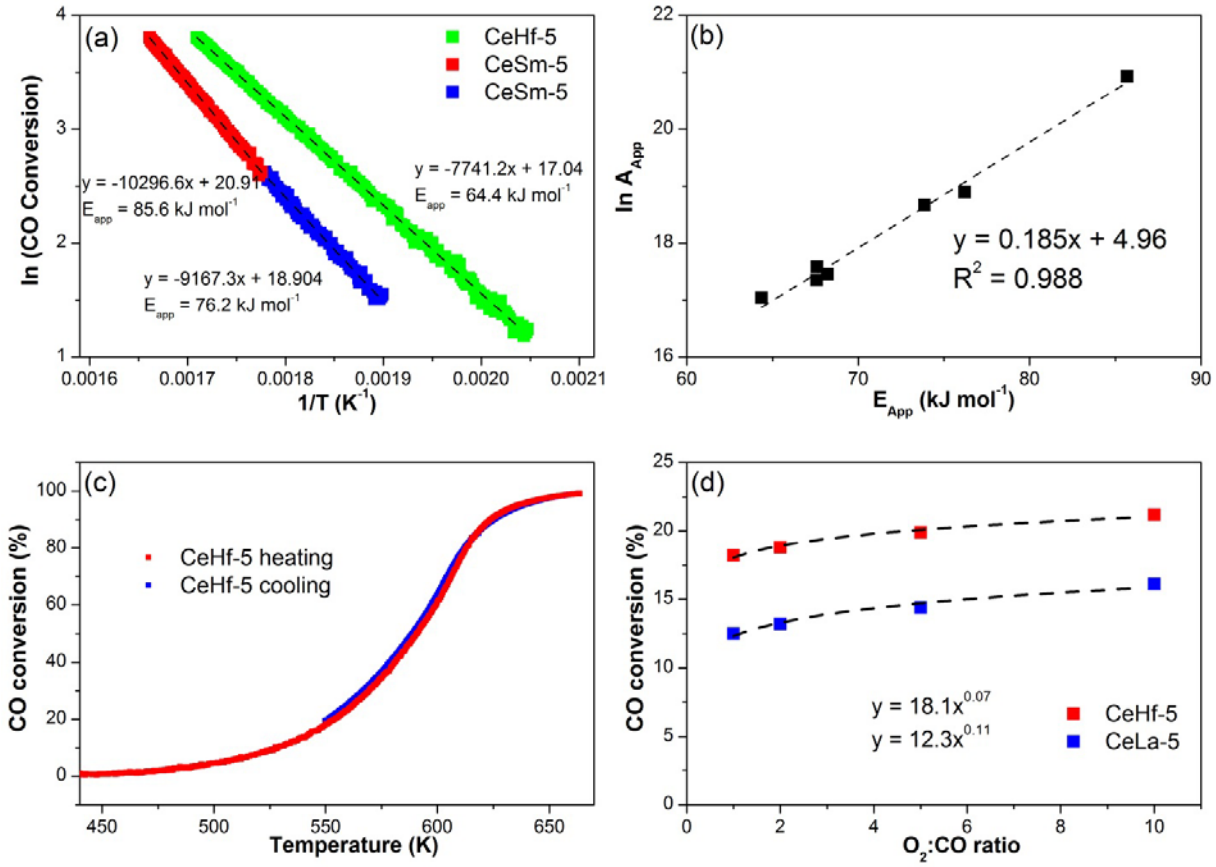

Figure S4. (a) Arrhenius plot for CO oxidation ($CO:O_2:He$ = 1:1:98) over CeSm-5 and CeHf-5. (b) Constable-Cremer relationship for CO oxidation over the studied catalysts. The Arrhenius parameters were determined in the smooth conversion range of ~5–40 % with excellent linear fit. The rate was plotted as "CO conversion" in the Arrhenius diagram. (c) CO conversion in heating and cooling section showing very little difference in reactivity over CeHf-5. At 550 K cooling was stopped and the feed O_2 content was varied. (d) Oxygen partial pressure dependence (at constant CO and total flow rate) with CeHf-5 and CeLa-5 at 550 K.

6. X-ray diffraction example; strain and size analysis

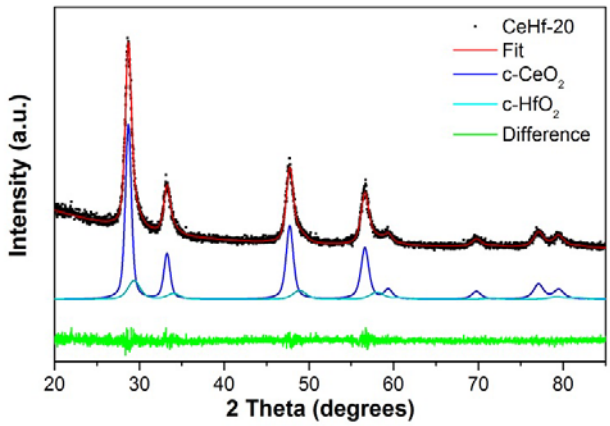

Figure S5. The XRD patter of CeHf-20 with its fitting showing the two cubic phases present.

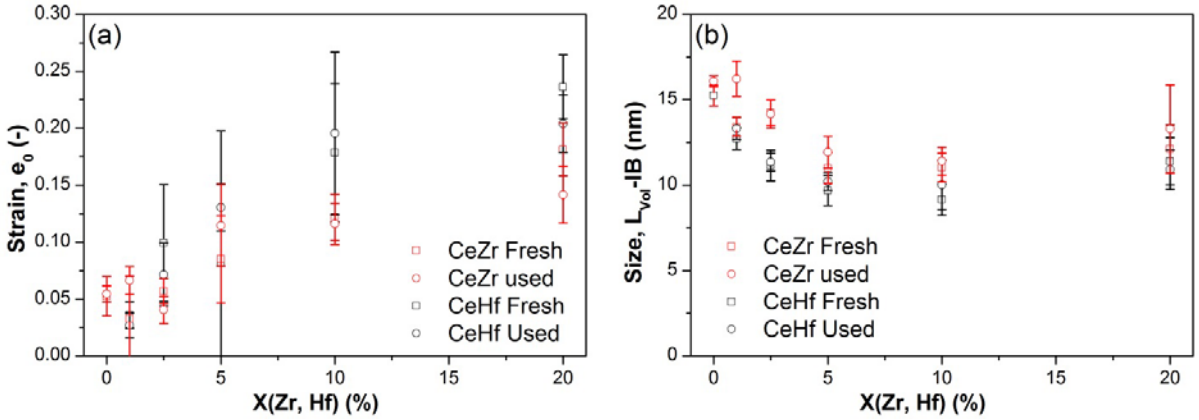

Figure S6. Strain (a) and crystallite size (b) as a function of Zr and Hf dopant concentration, as derived by the Double-Voigt pattern analysis.[6] Error bars correspond to ±3-times the estimated standard uncertainties.

7. Additional DFT results

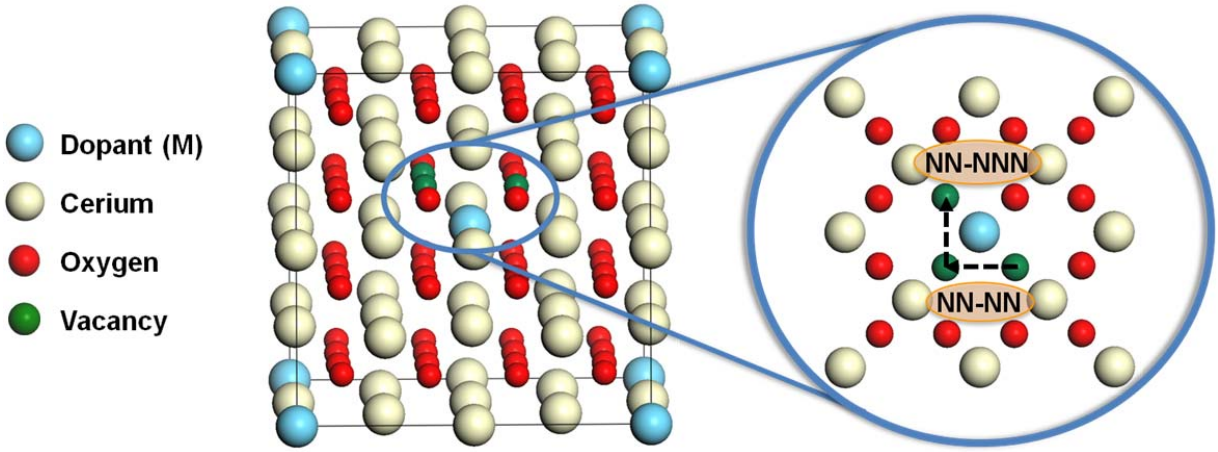

Figure S7. Side and top views of the calculated diffusion barriers for the oxygen vacancy in the M-doped-CeO_2(111) surface (M = Hf, La). Notice that when moving the vacancy a rearrangement of the associated electrons takes place.

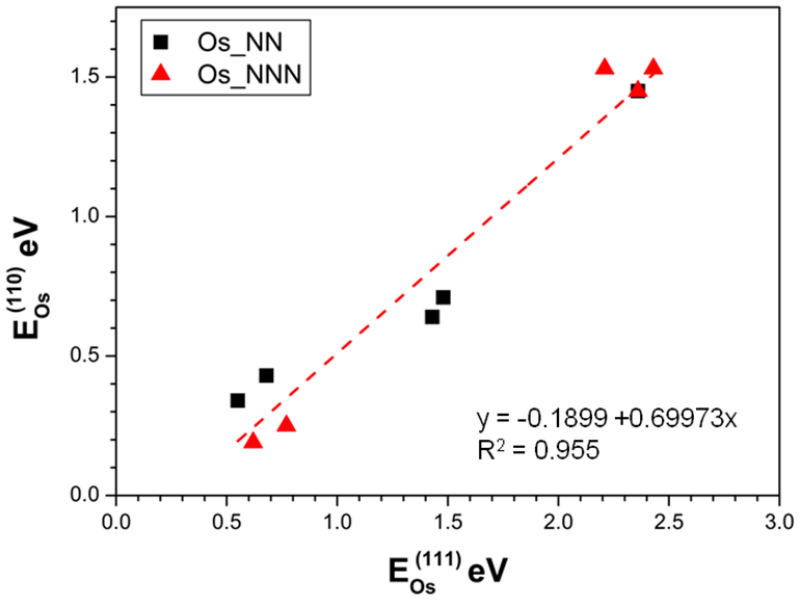

Figure S8. Plot of the calculated oxygen vacancy formation energy for the M-doped-CeO_2(110) surface versus the M-doped-CeO_2(111) surface.

Table S1. Calculated formation energy (in eV) of an oxygen surface defect in a p(3x3) $CeO_2(111)$ surface imposing a ferromagnetic (FM) and an antiferromagnetic (AFM) spin states:

O-defect	$\lvert\Delta E_{FM} - \Delta E_{AFM}\rvert$
O_s	< 0.01

Table S2. Calculated formation energies of an oxygen surface defect in a p(3x3) $CeO_2(111)$ surface, $\Delta E_{Os}^{(111)}$ in eV, with different locations of the pair of Ce^{3+} ions. In parenthesis, reported values for comparison:

Ce^{3+} positions[a]	$\Delta E_{Os}^{(111)}$	$\Delta E_{Os}^{(111)}$ ref. [7]	$\Delta E_{Os}^{(111)}$ ref. [8][b]
1_1-1_1	2.36	2.22	-
1_1-2_1	2.28	2.16	2.35
2_1-2_5	2.07	-	2.28

[a]The notation n_m implies a cation position in the *n*th shell of cations surrounding the defect, and *m* is the cationic layer counted from the surface. [b]For a p(2x2) cell (3x3x1 *k* points) and cutoff 400 eV.

Table S3. Calculated formation energy of an oxygen surface defect in a p(3x3) $CeO_2(111)$ surface, $\Delta E_{Os}^{(111)}$ in eV, with and without adding a U_{eff} term for the O(2p) states:

Ce^{3+} positions[a]	U_{eff} O(2p) states	$\Delta E_{Os}^{(111)a}$
1_1-1_1	0.0	2.36
1_1-1_1	7.0	1.74

[a]The energy difference of ~0.5 eV between the calculation with and without adding the U_{eff} term to O(2p) states is in good agreement with the 0.3-0.4 eV reported value in ref. [9].

Table S4. Relevant distances (in Å) for the $CeO_2(111)$ surface with no oxygen defects, and the $CeO_2(111)$ and M_s-doped-$CeO_2(111)$ (M = Hf, La) surfaces with an oxygen surface defect.

Surface	O-defect	Ce-Ce	Ce-M	Ce-O	M-O
CeO_2	-	3.886[a]	-	2.382	-
CeO_2-O_s	O_s	4.192[b] 4.244[c] 4.248[c]	-	2.420[f]/2.447[f] 2.420[f]/2.449[f] 2.276[g]/2.284[g]	-
CeHf-O_s-NN	O_s-NN	4.095[b]	4.273[d]	2.401[f]/2.436[f]	2.157
CeLa-O_s-NN	O_s-NN	4.266[c]	4.194[d]/4.263[e]	2.415[f]/2.442[f] 2.299[g]/2.294[g]	2.419/2.451

[a]Two Ce^{4+} cations. [b]Two Ce^{3+} cations. [c]Two Ce^{3+} and Ce^{4+} cations. [d]Ce^{3+} and M cations. [e]Ce^{4+} and M cations. [f]Ce^{3+} cation and an adjacent oxygen atom close to the defect. [g]Ce^{4+} cation and an adjacent oxygen atom close to the defect.

Table S5. Calculated polaron energy, E_{pol} in eV, oxygen diffusion barriers, E_a in eV for different M-doped bulk structures. Notice that when moving the anions a homogeneous distribution of dopants is employed. NN: nearest neighbor, NNN: next nearest neighbor, >NNN: further away from M.

Diffusion path	E_{pol}	E_a NN-NN	E_a NN-NNN	E_a >NNN
CeO_2	0.27	0.34	0.34	0.34
CeHf	0.17	0.06	0.14	0.19
CeLa	0.09	0.43	0.22	0.38

REFERENCES

1 Révay, Z.; Belgya, T.; Szentmiklósi, L.; Kis, Z.; Wootsch, A.; Teschner, D.; Swoboda, M.; Schlögl, R.; Borsodi, J.; Zepernick, R. *Anal. Chem*. **2008**, *80*, 6066–6071.

2 Revay, Z. *Anal. Chem.* **2009**, *81*, 6851–6859.

3 Eichelbaum, M.; Stößer, R.; Karpov, A.; Dobner, C.-K.; Rosowski, F.; Trunschke, A.; Schlögl, R. *Phys. Chem. Chem. Phys.* **2012**, *14*, 1302–1312.

4 Kajfez, D. *IEEE Trans. Microw. Theory Tech.* **1994**, *42*, 1149–1153.

5 Landau, L. D.; Lifshitz, E. M. *Electrodynamics of continuous media*, Pergamon Press: New York, **1960**; Looyenga, H. *Physica,* **1965**, *31*, 401–406.

6 Balzar, D. (1999): Voigt-function model in diffraction line-broadening analysis. - Microstructure Analysis from Diffraction, edited by R. L. Snyder, H. J. Bunge, and J. Fiala, International Union of Crystallography, 1999.

7 Jerratsch, J.-F.; Shao, X.; Nilius, N.; Freund, H.-J.; Popa, C.; Ganduglia-Pirovano, M. V.; Burow, A. M.; Sauer, J. *Phys. Rev. Lett.* **2011**, *106*, 246801.

8 Murgida, G. E.; Ganduglia-Pirovano, M. V. *Phys. Rev. Lett.* **2013**, *110*, 246101.

9 Yeriskin, I.; Nolan, M.; *J. Phys. Condens. Matter*, **2010**, *22*, 135004.